MOX-Report No. 46/2015

Emerging morphologies in round bacterial colonies: comparing volumetric versus chemotactic expansion

Giverso, C.; Verani, M.; Ciarletta P.

MOX, Dipartimento di Matematica
Politecnico di Milano, Via Bonardi 9 - 20133 Milano (Italy)

mox-dmat@polimi.it http://mox.polimi.it

Emerging morphologies in round bacterial colonies: comparing volumetric versus chemotactic expansion

Chiara Giverso[1,2], Marco Verani[1] and Pasquale Ciarletta[1,2]

September 24, 2015

[1] MOX– Modellistica e Calcolo Scientifico
Dipartimento di Matematica "F. Brioschi"
Politecnico di Milano, Milano, Italy
chiara.giverso@polimi.it

[2] Fondazione Centro Europeo Nanomedicina
Piazza Leonardo da Vinci, 32, 20133 Milano, Italy

Keywords: bacteria colony growth, branching instability, bacterial chemotaxis, volumetric growth

Abstract

Biological experiments performed on living bacterial colonies have demonstrated the microbial capability to develop finger-like shapes and highly irregular contours, even starting from an homogeneous inoculum. In this work, we study from the continuum mechanics viewpoint the emergence of such branched morphologies in an initially circular colony expanding on the top of a Petri dish coated with agar. The bacterial colony expansion, based on either a source term, representing volumetric mitotic processes, or a non-convective mass flux, describing chemotactic expansion, is modelled at the continuum scale. We demonstrate that the front of the colony is always linearly unstable, having similar dispersion curves to the ones characterizing branching instabilities. We also perform finite element simulations, which not only prove the emergence of branching, but also highlight dramatic differences between the two mechanisms of colony expansion in the nonlinear regime. Furthermore, the proposed combination of analytical and numerical analysis allowed studying the influence of different model parameters on the selection of specific patterns. A very good agreement has been found between the resulting simulations and the typical structures observed in biological assays. Finally, this work provides a new interpretation of the emergence of branched patterns in living aggregates, depicted as the results of a complex interplay among chemical, mechanical and size effects.

1 Introduction

Bacteria have long been considered as simple unicellular organisms that grow and live independently from each other [52]. However, in the last decades, many experimental and theoretical works have shown that, regardless of their small size and quite primitive structure, they display a high behavioral complexity. In fact, bacteria can carry out collective strategies for adaptation and survival, and they can also collaborate, forming colonies in which individual behaviours and abilities are adjusted for the convenience of the whole population [5, 13, 42, 52]. Accordingly, when a small number of bacteria is inoculated on a Petri-dish with an appropriate culture medium, they exhibit coordinate behaviors and they collectively grow setting-up structured and complex colonies. Such colonies might differ in size, form and functions according to the bacterial species and to the environmental conditions [42]. For instance, a wide variety of morphological patterns is reported from experiments using Bacillus Subtilis [14,27,33,41,42], ranging from disk-like colonies to dense branched morphology, including diffusion-limited aggregation (DLA)-like patterns, compact Eden-like structures [21] and concentric ring-like morphologies.

During the course of evolution, bacteria have developed sophisticated means to communicate both among them and with the extracellular environment [5,29], in order to adapt in response to changes in environmental conditions. These communicative strategies

include long- and short-range chemical signalling and contact-mediated mechanical interactions [4, 5]. The chemical communication is based on the bacterial secretion of chemicals and on the microbial ability of binding, through membrane receptors, specific chemical molecules that can be either generated by other bacteria belonging to the same colony or they can be externally-generated [5]. Furthermore, bacteria do not only sense biochemical signals but they also respond to physical factors, thanks to their membrane receptors and mechanically gated channels. The conversion of the mechanical stimulus into a biological response, which is commonly referred to as mechano-transduction, is a crucial feature to interact both with the other bacteria in the colony and with the external environment [31]. The chemical and mechanical interactions thus affect the bacterial behaviour through complex intracellular mechanisms involving signal transduction pathways and gene expression dynamics [38]. This feedback mechanisms lead to the coordination of a large number of bacteria in space and time, through either synchronization or differentiation of the different individuals in the colony [4, 52]. One result of this cooperative behavior is the formation of complex spatio-temporal patterns during the evolution of the colony, which have attracted the interest of a broad multidisciplinary community of scientists for a long time [10, 12, 49].

Indeed, bacteria capability to grow elaborate branching patterns, starting from an initially homogeneous microbial monolayer, was first studied by Fujikawa and Matsushita (1989), who postulated that nutrient diffusion and consumption was driving the instability of the expanding front. When plated on a Petri dish, the nutrients (e.g. peptone) contained in the culture medium diffuses towards the colony, providing the influx of energy needed by bacteria in order to proliferate, move and perform any other metabolic process. Nutrient consumption creates a gradient in the chemical concentration, that plays a key role in microbial dynamics [10–12, 27, 33, 41–43, 57]. Precisely, many biological experiments [2, 10, 12, 29, 47] pointed out that bacteria are not only able to perform a random-walk-like motion but they can also direct their movements in response to external chemical signals, a process called *chemotaxis*. Thus, bacterial movements resemble a random walk in a uniform environment, in which relatively straight swim phases alternate with random tumbles of the flagella reorienting the micro-organism. Conversely, in the presence of an external chemical gradient bacteria direct their motion by reducing the tumbling frequency of their flagella, when they move up the gradient of a chemo-attractant or, equivalently, down the gradient of a chemo-repulsive substance [2]. In order to perform both undirected and directed motions, bacteria need to move on the underlying agar, swimming in the fluid on the top of it. This thin layer of lubricant liquid might be collectively produced by the cells themselves, but also drawn from the agar during bacterial expansion [10, 29]. Thus, thanks to in-vitro experiments, bacteria expansion has been demonstrated to rely on the nutrient availability and on the bacteria capability to migrate on the top of the agar, which in turn depends on the mechanical properties of the underlying agar and on the properties and the quantity of this fluid on the top of it [10, 12, 35].

Nevertheless, understanding the collective growth and motion of micro-organisms in response to chemicals and mechanical cues is a challenge not only from the experimental point of view, but also from the mathematical and bio-mechanical perspectives, since it

requires combining biological information with the mathematical theories of nonlinear dynamics and the physics and mechanics of non-equilibrium processes. In particular, many mathematical models have been proposed in the last decades to describe pattern formation in microbial colonies, starting from the observation that the bacterial patterns are similar to the ones found in some non-living systems [8, 9]. Existing mathematical models can be divided into two main categories:

- discrete/hybrid models, characterized by a discrete representation of the single moving entities and a continuous description of the chemicals (e.g. the communicating walkers model proposed by Ben-Jacob et al. (1998) and by Ben-Jacob and Levine (2006), or the agent-based model used by Bonachela et al. (2011)). Even though these models allow a direct simulation of the single agents, that consume nutrients, reproduce, move randomly or in response to chemical fields, they are computationally limited in the number of individuals that can be simulated;

- continuous models, in which the bacterial colony, the nutrients and all the other factors involved in the process, are represented via their averaged densities [11, 33, 35, 40, 41, 43, 56]. Among them, there are reaction-diffusion (RD) models, so called because the spatial and temporal evolution of the species' densities is described by a systems of coupled reaction-diffusion equations [43]. Such models were able to reproduce accurately not only disk-like patterns, but also branched ones. In particular, disk-like patterns have been recovered using a two-dimensional Fisher equation for the bacterial population [42, 56]. Instabilities here rely on the introduction of a non-linear diffusion coefficient [33, 43] or to a limitation in the rate of transition from the bacteria active (i.e. motile and proliferative) state to the passive one [41]. Such models may also include a chemotactic term [15,40], combining signals from a chemorepellent and a chemoattractant (to prevent overcrowding, while keeping the cells together).

Even though both continuous and hybrid models have been proved to qualitatively reproduce some bacterial patterns, most of these researches focused on diffusing chemicals as the major guide of the whole phenomenon, without considering proper mechanical balance laws. However, recent works [3, 16, 28, 32, 53] have demonstrated the paramount importance of describing growth and migration in biological processes using the proper continuum mechanics framework. Thus, bio-mechanical considerations cannot be neglected in order to describe the expansion and the consequent formation of complex morphologies in bacterial colonies.
Some recent attempts to incorporate a mechanical description in bacterial models can be found, for instance, in the work of Farrell et al. (2013), where some mechanical interactions are modelled at the cellular scale in a two-dimensional bacterial colony, and in the paper of Dockery and Klapper (2001), where the formation of finger-like structures during the volumetric growth of a planar biofilm is investigated, without considering the effect of chemotaxis.

In the present work, we will focus on determining the role of both chemical and mechanical interactions on the pattern formation of an expanding circular bacterial colony. The mechanical description is here presented from a continuum viewpoint, describing the friction arising from the interaction between the colony and the substrate, and the surface tension acting at the boundary of the colony, due to the collective interaction with the biopolymers inside the surrounding liquid environment [23].
The growth and chemotactic mobility of the biological colony, coupled with the diffusion and consumption of nutrients provided by the agar, are described using a continuum mechanical model at the macroscopic scale. The bacterial growth within a Petri dish is described as a free-boundary problem, in which the growth of the colony is driven by either a pure volumetric mass production inside the body or a non-convective mass flux due to chemotaxis.
In Section 2, we first present the mathematical model for describing the expansion mechanisms of a bacterial cluster. Then, in Section 3, we perform a linear stability analysis for a quasi-static bacterial expansion. In Section 4, we perform numerical simulations to analyze the dynamics of pattern formation in the nonlinear regime. Finally, the main achievements of this work, with a particular focus on their significance for biological problems, are discussed in Section 5.

2 Mathematical model

Let us model the bacterial colony as a two dimensional continuum body, whose expansion over time is described by a moving free boundary. A continuous model is a suitable tool since no gaps appear in the expanding culture and the average pore size of the underlying agar is smaller than the typical dimension of the single bacterium [33, 41]. Moreover, the growth of the colony on the top of the agar surface can be approximated as two-dimensional in the reported experimental conditions [29, 33, 40, 41].
The bacteria colony is modelled to occupy a region denoted with $\Omega^-(t)$ (see Fig. 1) surrounded by a spatial domain $\Omega^+(t)$, filled with an inviscid fluid, which represents the thin layer of lubricant observed on the top of the agar in biological assays [10, 12]. The moving interface between the colony and the external environment is denoted with $\partial\Omega^-(t)$ (see Fig. 1).
The nutrients can diffuse through the agar inside the inviscid fluid layer on top of it, with diffusion coefficient D_n, from the fixed outer boundary of the Petri dish $\partial\Omega^+$ and it is consumed by the living material in $\Omega^-(t)$, with an uptake rate γ_n. Thus, the the 2D homogenized concentration per unit volume of this generic chemical, indicated with $n(\mathbf{x}, t)$, obeys the following reaction-diffusion equation

$$\dot{n}(\mathbf{x},t) = \begin{cases} D_n \nabla^2 n(\mathbf{x},t) - \gamma_n n(\mathbf{x},t) & \text{in } \Omega^-(t)\,, \\ D_n \nabla^2 n(\mathbf{x},t) & \text{in } \Omega^+(t)\,. \end{cases} \tag{1}$$

Typical values of the diffusion coefficient D_n range from $10^{-12}\,\mathrm{m}^2/\mathrm{s}$ to $10^{-9}\,\mathrm{m}^2/\mathrm{s}$ [20, 24, 29, 59], whereas the uptake rate γ_n is in the order of $10^{-4} - 10^{-3}\,\mathrm{s}^{-1}$ [29, 58].

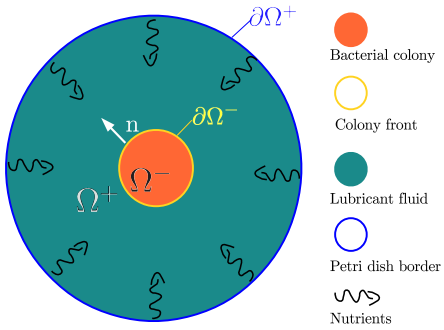

Figure 1: Scheme representation of the domain used for the analytical and numerical analysis. At time $t = 0$, $\Omega^-(0)$ is a circle, with radius $R^*(0) = R_0^*$. The fixed border $\partial\Omega^+$ represents the outer radius of the Petri dish.

In principle, we remark that the uptake rate γ_n should depend on the bacterial density, although, in the following, it will be considered homogeneous and constant over time. The diffusing chemical notably affects the growth of single individuals in the colony and it directs cell movements, through chemotaxis [2, 37]. Hence, we consider both a volumetric mass supply, Γ, and a non-convective mass flux term, $\mathbf{m}$, for describing the process of mass accretion inside the living aggregate. Accordingly, the mass balance equation representing the evolution of the actual bacterial density, ρ, reads

$$\frac{d\rho}{dt} + \rho\nabla\cdot\mathbf{v} = \Gamma + \nabla\cdot\mathbf{m}\,. \tag{2}$$

Since growth processes and mass transport phenomena in living materials are driven by the local concentration of chemicals, proper constitutive equations for the mass source term and the mass flux vector appearing in Eq. (2) should take into account nutrient availability. Thus, we will consider the two different situations:

- the expansion of the colony is driven by non-convective mass fluxes and no mitotic processes occur inside the volume, i.e. $\Gamma = 0$. Neglecting the random-motion of bacteria with respect to the directional one [2], a simple dissipative constitutive law for $\mathbf{m}$ can be taken in the form of a chemotactic term [34], i.e. $\mathbf{m} = \chi\rho\nabla n$, where χ is the chemotactic coefficient, experimentally measured in the order of $3.75 - 188\cdot 10^{-5}\,\mathrm{cm}^2/(\mathrm{s}\cdot\mathrm{mM})$ [24, 54]. Since the mass flux $\mathbf{m}$ describes chemotactic expansion of the colony towards higher concentration of nutrients, in the following we will refer to this case as the *chemotactic growth model*;

- the mass production occurs inside the volume of the material, without non-convective mass exchanges, i.e. $\mathbf{m} = 0$. The volumetric mass supply Γ can be taken proportional to the nutrient concentration and the bacterial density [33], i.e. $\Gamma = K_\gamma\rho n$, where K_γ is the bacterial reproduction rate per unit of nutrient concentration (that was estimated to be in the order of $K_\gamma = 6\cdot 10^{-5}\mathrm{l}/(\cdot\mathrm{s})$ in [29]). This situation is later referred to as *bulk* or *volumetric growth model*.

In the following, both mass source terms will be modeled using linear constitutive equation with the aim to study the linear stability of the quasi-stationary solution without introducing non linearities in the governing equations.
While the volumetric mass production and the mass flux vector appearing in Eq. (2) are related to chemical properties of the system, the physical velocity field should be linked to the mechanical properties of our material. Considering that the living aggregate can be macroscopically described by a Newtonian fluid moving at low Reynolds numbers and under the assumption of a very slow growth process, the Stokes equations for a two-dimensional flow of a thin film of viscous fluid reduce to a relation similar to the classical Darcy's law [30, 50], that couples the velocity $\mathbf{v}$ to the pressure field p through

$$\mathbf{v} = -K_p \nabla p \,, \tag{3}$$

where the typical permeability coefficient of the material, K_p, is related, in this context, to the inverse of the friction between the colony and the substrate and it represents the motility of the colony. Then, we assume the two-dimensional incompressibility of the biological matter, which is mostly composed by water, i.e. $d\rho/dt = 0$ in Eq. (2). This assumption corresponds to consider an initial condition where the almost flat colony is no longer swelling in the transverse direction, and starts expanding whilst keeping an approximately constant thickness [51]. The relation between the pressure p and the nutrient concentration n is obtained introducing the Darcy's law (3) in the mass balance (2) and substituting the constitutive relations for $\mathbf{m}$ and Γ. Accordingly, for a homogeneous bacterial colony, taking $\Gamma = 0$ and $\mathbf{m} = \chi\rho\nabla n$ for the *chemotactic growth model* we have

$$\nabla^2 p = -\frac{\chi}{K_p}\nabla^2 n \quad \text{in } \Omega^-(t) \,, \tag{4}$$

whereas for the *bulk growth model*, the constitutive assumptions $\Gamma = K_\gamma \rho n$ and $\mathbf{m} = 0$ lead to

$$\nabla^2 p = -\frac{K_\gamma}{K_p} n \quad \text{in } \Omega^-(t). \tag{5}$$

In summary, the coupling of Eq. (1) with Eq.(4) (resp. Eq.(5)), describes the macroscopic evolution of the system, under the condition of a *chemotactic growth model* (resp. *volumetric growth model*).
These systems of partial differential equations must be complemented by a set of boundary conditions (BCs). In particular, we assume for both systems that the Young-Laplace equation holds at the free interface $\partial\Omega^-(t)$. Thus, calling C the local curvature of the free boundary, being σ_b the surface tension of the interface and p_0 the constant outer pressure, the mechanical equilibrium is guaranteed by the condition

$$p = p_0 - \sigma_b C \qquad \text{on } \partial\Omega^-(t) \,. \tag{6}$$

The surface tension of the colony arises from the collective interaction between the bacteria at the border and the biopolymers in the liquid environment [23], forming a

Table 1: Dimensionless equation systems for the *chemotactic growth model* and the *bulk growth model*. The dimensionless nutrients concentration is denoted with $\bar{n}$ and the dimensionless pressure with $\bar{p}$.

Chemotactic growth model $(\Gamma = 0\,, \mathbf{m} = \chi\rho\nabla n)$	**Bulk growth model** $(\Gamma = K_\gamma \rho n\,, \mathbf{m} = 0)$
Governing equations:	
$\dot{\bar{n}} = \begin{cases} \nabla^2\bar{n} - \bar{n} & \text{in } \Omega^-(t) \\ \nabla^2\bar{n} & \text{in } \Omega^+(t) \end{cases}$	
$\nabla^2\bar{p} = -\beta_1\nabla^2\bar{n} \quad \text{in } \Omega^-(t)$	$\nabla^2\bar{p} = -\beta_2\bar{n} \quad \text{in } \Omega^-(t)$
Dimensionless BCs	
$\bar{p}\vert_{\partial\Omega^-} = \bar{p}_0 - \sigma\bar{C}$	
$[\![\bar{n}]\!]\vert_{\partial\Omega^-} = 0$	
$[\![\nabla\bar{n}\cdot\mathbf{n}]\!]\vert_{\partial\Omega^-} = 0$	
$\frac{\mathrm{d}\bar{\mathbf{x}}_{\partial\Omega^-}}{\mathrm{d}t}\cdot\mathbf{n} = \bar{\mathbf{v}}_{\partial\Omega^-}\cdot\mathbf{n}$	
$\bar{n}\vert_{\partial\Omega^+} = 1$	
Dimensionless parameters	
$\beta_1 = \frac{\chi n_c}{D_n}$	$\beta_2 = \frac{K_\gamma n_c}{\gamma_n}$
$\sigma = \sigma_b \frac{K_p \gamma_n^{1/2}}{D_n^{3/2}}$	

crosslinked structure all around the border of the colony [10, 35].
Moreover, the compatibility condition at the free interface imposes

$$\frac{\mathrm{d}\mathbf{x}_{\partial\Omega^-}}{\mathrm{d}t}\cdot\mathbf{n} = \mathbf{v}_{\partial\Omega^-}\cdot\mathbf{n} \qquad \text{on } \partial\Omega^- \tag{7}$$

where $\mathbf{n}$ is the outward normal vector at the boundary. The continuity for the nutrient concentration and flux can be assumed in absence of an interfacial structure, so that

$$[\![n]\!]\vert_{\partial\Omega^-} = 0\,, \tag{8}$$

$$[\![\nabla n\cdot\mathbf{n}]\!]\vert_{\partial\Omega^-} = 0\,, \tag{9}$$

where $[\![(\cdot)]\!]\vert_{\partial\Omega^-}$ denotes the jump of the quantity between brackets across the boundary $\partial\Omega^-(t)$. Finally, we will consider two kinds of boundary conditions at the outer boundary of the Petri dish, corresponding to two different biological experimental settings. First, we will consider that the concentration of nutrients at the fixed external boundary remains constant over time, i.e.

$$n\,\vert_{\partial\Omega^+} = n_{out} \qquad \text{on } \partial\Omega^+\,, \tag{10}$$

which corresponds to the case in which nutrients are continuously added in the agar at the border of the Petri dish, so that their concentration is kept constant. This approximation also holds for small initial colonies growing far enough from the outer border of the Petri dish. Then, we will analyze the case in which the nutrients are introduced at the outset and no flux occurs at the edge of the dish, i.e

$$\nabla n \cdot \mathbf{n} \mid_{\partial\Omega^+} = 0 \qquad \text{on } \partial\Omega^+ \,, \tag{11}$$

that is the situation most commonly found in biological experiments. In the following we will work with dimensionless equations, obtained writing the system of Eqs. (1)-(4) and (1)-(5) in terms of the dimensionless variables, denoted with barred symbols (e.g. $\bar{n}$ denotes the dimensionless nutrients concentration whereas $\bar{p}$ indicates the dimensionless pressure), with respect to the following characteristic length l_c, time t_c, velocity v_c, pressure p_c and chemical concentration n_c

$$l_c = \sqrt{D_n \gamma_n^{-1}} \,, \quad t_c = \gamma_n^{-1} \,, \quad v_c = \sqrt{D_n \gamma_n} \,,$$

$$p_c = D_n K_p^{-1} \,, \quad n_c = n_{out}(t=0) \,.$$

Considering the typical biological values reported in literature for D_n [20,24,29,59] and γ_n [29, 58], we have a characteristic time in the range of $16 - 166\,\mathrm{min}$ and a diffusive length l_c that can vary between $100\,\mu\mathrm{m}$ and $3\,\mathrm{mm}$, which is much smaller than the $44\,\mathrm{mm}$-radius of the typical Petri dish used in the experiments performed on bacteria. The two dimensionless systems of equations are reported in Table 1. Interestingly, in each system only two dimensionless parameters appear: $\sigma = \sigma_b K_p \gamma_n^{1/2} D_n^{-3/2}$ in both models and either $\beta_1 = \chi n_c D_n^{-1}$ in the *chemotactic growth model* or $\beta_2 = K_\gamma n_c \gamma_n^{-1}$ in the *volumetric growth model*. The dimensionless parameter β_i (with $i = 1$ in the *chemotactic growth model* and $i = 2$ in the *bulk growth model*) represents the ratio between the energy required for the expansion of the colony (i.e. either the energy associated to the chemotactic expansion in the *chemotactic growth model* or the energy supply for the mass production process in the *volumetric growth model*) and the energy provided by the nutrients (i.e. either the energy associated to the diffusion of nutrients in the *chemotactic growth model* or the energy provided by their uptake in the *volumetric growth model*). On the other hand, the parameter σ depends on the surface tension of the colony, on the permeability of the medium and on the diffusion coefficient of the chemicals. In particular, the permeability coefficient of the medium can be related through $K_p = l_c/\zeta$ to the friction ζ between the colony and the substrate (ζ is in the order of $1 - 10^2\,\mathrm{nNs}/(\mu\mathrm{m}^3)$, as found in Ziebert and Aranson (2013)). Accordingly , the dimensionless parameter σ becomes the ratio between the surface tension of the bacterial colony and the product between the colony-substrate friction and the diffusion coefficient, $\sigma = \sigma/(D_n\zeta)$.
In the following sections, we will omit the barred notation for dimensionless quantities for the sake of simplicity.

3 Linear stability analysis

In this section we will study the stability of the quasi-stationary solution, obtained assuming that the diffusive process is faster than the motion of the colony border, so that it is possible to drop the time derivative in Eq. (1). Both the *chemotactic growth* and the *bulk growth model* introduced in Section 2 will be considered. The assumption of a quasi-stationary evolution of the colony can be valid in those experimentally observed situations [33, 41] in which the growth of the colony occurs slowly enough to consider the diffusive equilibrium for the nutrients. In particular, we specialize our analysis to the case of a circular colony, i.e.

$$\Omega^-(t) = \{(r,\theta) : \, r < R^*(t), 0 < \theta \leq 2\pi\} \, ,$$

with free border $\partial\Omega^-(t) : \, r = R^*(t)$, immersed in an external domain,

$$\Omega^+(t) = \{(r,\theta) : \, R^*(t) < r \leq R_{out}, 0 < \theta \leq 2\pi\} \, ,$$

where $R^*(t)$ is the dimensionless radial position of the free boundary and R_{out} is the external dimensionless radius.

3.1 Quasi-stationary solution

The existence of a non-null quasi-stationary solution for the nutrients is guaranteed only under the assumption that the boundary condition (10) holds (as the only stationary solution by applying BC (11) would correspond to a null concentration everywhere). Thus, the quasi-stationary solution n^* of Eq. (1) fulfilling the internal boundary conditions (8) and (9) reads

$$n^*(r,t) = \begin{cases} n_0 \dfrac{I_0(r)}{I_0(R^*)} & \text{if } r < R^* \\ n_0 + (1-n_0)\dfrac{\log\left(\dfrac{r}{R^*}\right)}{\log\left(\dfrac{R_{out}}{R^*}\right)} & \text{if } R^* < r \leq R_{out}, \end{cases} \tag{12}$$

where $n_0 = n_0(t) = \left(1 + \dfrac{I_1(R^*)}{I_0(R^*)} R^* \log\left(\dfrac{R_{out}}{R^*}\right)\right)^{-1}$ is the nutrient concentration at the moving interface and $I_m(r)$ is the modified Bessel function of the first kind of order m, evaluated in r. The expression for $n_0(t)$ can be found imposing the continuity condition (9). Once the quasi-stationary concentration of the nutrient is given, it is possible to solve either Eq. (4) or Eq. (5), depending on the chosen model, and obtain the spatial evolution of the pressure field. Given the boundary condition (6) and imposing the boundedness of the quasi-stationary pressure field p^*, both solutions are given by

$$p^*(r,t) = -\beta_i \left(n^*(r,t) - n_0(t)\right) + p_0 + \frac{\sigma}{R^*(t)} \, . \tag{13}$$

Through Eq. (3), it is then possible to calculate the quasi-stationary velocity of the front, which is directed along the radial direction for symmetry considerations, i.e. $\mathbf{v}^* = v_r^* \mathbf{e}_r$, with

$$v_r^*(R^*) = \beta_i n_0 \frac{I_1(R^*)}{I_0(R^*)} \,. \tag{14}$$

Eq. (14) can be integrated numerically to determine the evolution of the colony border over time. Interestingly, we observe that the normal velocity of the colony interface does not depend on the permeability coefficient K_p, but it only depends on the parameter β_i. Thus, Eq. (14) allows to check the validity of the quasi-stationary assumption by comparing the characteristic times of colony growth and nutrient diffusion. In those cases in which the quasi stationary assumption cannot be formulated, the non stationary solution should be approached. However, in this case the treatise would be far more complex, since the shape of the boundary cannot be fixed a priori, but should be derived a posteriori solving the whole set of coupled PDEs [48].

3.2 Perturbation of the quasi-stationary solution

Let us now consider a perturbation of the free-boundary with *amplification rate* (or *time-growth rate*) equal to $\lambda \in \mathbb{R}$ and spatial wave-number $k \in \mathbb{N}^+$, i.e.

$$R(\theta, t) = R^*(t) + \varepsilon e^{\lambda t} \cos(k\theta) \,. \tag{15}$$

with $|\varepsilon| \ll 1$. For physical consistency, the variations of n and p from the quasi-stationary solution, n^* and p^* are assumed in the form

$$n(r, \theta, t) = n^*(r, t) + \varepsilon n_1(r) e^{\lambda t} \cos(k\theta) \,, \tag{16}$$

$$p(r, \theta, t) = p^*(r, t) + \varepsilon p_{1,i}(r) e^{\lambda t} \cos(k\theta) \,, \tag{17}$$

where, as before, $i = 1$ in the *chemotactic growth model* and $i = 2$ in the *volumetric growth model*. Using (1), we know that n_1 is the solution of both systems of ODEs

$$\begin{aligned} r^2 n_1''(r) + r n_1'(r) - \left(k^2 + (\lambda+1) r^2\right) n_1(r) &= 0 \\ \text{if } r &< R^*(t) \,, \end{aligned} \tag{18}$$

$$\begin{aligned} r^2 n_1''(r) + r n_1'(r) - \left(k^2 + \lambda r^2\right) n_1(r) &= 0 \\ \text{if } R^*(t) < r &< R_{out} \,, \end{aligned} \tag{19}$$

where primes denote derivatives on r. In the following we will denote with n_1^- the solution of (18) and with n_1^+ the solution of (19).

In particular, it is possible to see that the nature of the solution of (18)-(19) changes with the value of the parameter λ. Calling $K_m(r)$ the modified Bessel function of the second kind of order m, evaluated in r, the solutions of (18)-(19) are:

- $n_1^-(r) = A I_k(\sqrt{\lambda+1} r)$ and $n_1^+(r) = B I_k(\sqrt{\lambda} r) + D K_k(\sqrt{\lambda} r)$, when $\lambda \neq \{0, -1\}$;

Table 2: Quasi-stationary solution for the concentration field in the region occupied by the bacterial colony.

Case	$n_1^-(r)$	
$\lambda \neq \{0,-1\}$	$AI_k(\sqrt{\lambda+1}r)$	$A = n_0 \dfrac{I_k(\sqrt{\lambda}R^*)K_k(\sqrt{\lambda}R_{out}) - K_k(\sqrt{\lambda}R^*)I_k(\sqrt{\lambda}R_{out})}{denA}$
		$denA = \sqrt{\lambda+1}I_{k-1}(\sqrt{\lambda+1}R^*)\left(I_k(\sqrt{\lambda}R_{out})K_k(\sqrt{\lambda}R^*) - K_k(\sqrt{\lambda}R_{out})I_k(\sqrt{\lambda}R^*)\right) +$
		$+\sqrt{\lambda}I_k(\sqrt{\lambda+1}R^*)\left(I_k(\sqrt{\lambda}R_{out})K_{k-1}(\sqrt{\lambda}R^*) + K_k(\sqrt{\lambda}R_{out})I_{k-1}(\sqrt{\lambda}R^*)\right)$
$\lambda = 0$	$A_0 I_k(\sqrt{\lambda+1}r)$	$A_0 = n_0 \dfrac{(R^{*2k} - R_{out}^{2k})}{denA_0}$
		$denA_0 = 2kR^{*2k-1}I_k(\sqrt{\lambda+1}R^*) - \sqrt{\lambda+1}\left(R^{*2k} - R_{out}^{2k}\right) I_{k-1}(\sqrt{\lambda+1}R^*),$
$\lambda = -1$	$A_1 r^k$	$A_1 = n_0 \dfrac{I_k(\sqrt{\lambda}R^*)K_k(\sqrt{\lambda}R_{out}) - K_k(\sqrt{\lambda}R^*)I_k(\sqrt{\lambda}R_{out})}{denA_1}$
		$denA_1 = 2kR^{*k-1}\left(I_k(\sqrt{\lambda}R_{out})K_k(\sqrt{\lambda}R^*) - K_k(\sqrt{\lambda}R_{out})I_k(\sqrt{\lambda}R^*)\right) +$
		$+R^{*k}\sqrt{\lambda}\left(I_k(\sqrt{\lambda}R_{out})K_{k-1}(\sqrt{\lambda}R^*) + K_k(\sqrt{\lambda}R_{out})I_{k-1}(\sqrt{\lambda}R^*)\right)$

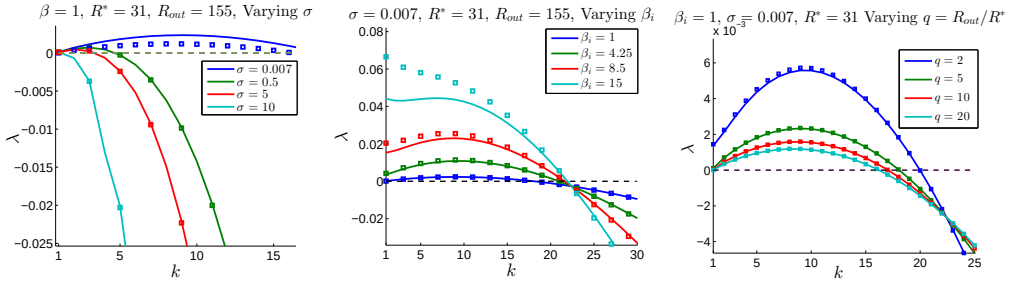

(a) (b) (c)

Figure 2: Dispersion diagrams for different values of the model parameters σ, β_i and $q = R_{out}/R_0^*$. The dots correspond to the numerical solution of the dispersion equations for $k \in \mathbb{N}$, $k \geq 1$ in the *volumetric growth model*, whereas the solid lines are obtained through interpolation of the discrete values of λ obtained with the *chemotactic growth model*.

- $n_1^-(r) = A_0 I_k(\sqrt{\lambda+1}r)$ and $n_1^+(r) = B_0 r^k + D_0 r^{-k}$, when $\lambda = 0$;
- $n_1^-(r) = Ar^k$ and $n_1^+(r) = B_1 I_k(\sqrt{\lambda}r) + D_1 K_k(\sqrt{\lambda}r)$, when $\lambda = -1$.

The coefficients appearing in the expression of $n_1^-(r)$ and $n_1^+(r)$ can be determined imposing the boundary conditions in (8), (9) and (10), being

$$[\![n_1]\!]|_{R^*} = 0, , \tag{20}$$

$$[\![\frac{\partial n_1}{\partial r}]\!]|_{R^*} = n_0 \, , \tag{21}$$

$$n_1^+(R_{out}) = 0 \, , \tag{22}$$

We report in Table 2 the solution of n_1^- and the values of A, A_0, A_1, as they will be useful in the definition of the dispersion relations.

The perturbed pressure field $p_{1,i}$ in Ω^-, can be determined from (4) when $i = 1$ or (5) when $i = 2$, that lead to

$$p_{1,1}(r) = E_1 r^k - \beta_1 n_1^-(r) \textit{ (chemotactic growth)} \tag{23}$$

and

$$\begin{aligned} p_{1,2}(r) &= \frac{\beta_2}{2k}\left[r^{-k}\int r^{k+1} n_1^-(r)dr - r^k \int r^{-k+1} n_1^-(r)dr\right] \\ &+ E_2 r^k \textit{ (volumetric growth)}. \end{aligned} \tag{24}$$

The constants E_1 and E_2 depends on the condition (6), that leads to

$$\begin{aligned} p_{1,i}(R^*) &= \sigma\frac{k^2-1}{R^{*2}} - \frac{\partial p^*}{\partial r}(R^*) = \\ &= \sigma\frac{k^2-1}{R^{*2}} + \beta_i n_0 \frac{I_1(R^*)}{I_0(R^*)}, \end{aligned} \tag{25}$$

considering only the first order terms. Finally, the dispersion equation

$$\lambda = -p^{*\prime\prime}(R^*) - p'_{1,i}(R^*), \tag{26}$$

is obtained from Eq. (7), neglecting the terms of order higher than the first. The dispersion equation (26) has the same form of the relation found for the rectilinear front on an infinite domain [17]. More details on the determination of the boundary condition for the perturbed pressure field (25) and on the theoretical derivation of the dispersion equation (26) can be found in the Appendix. The specific expressions for the dispersion equations are reported in the Appendix (see Table 3 for the *chemotactic growth model* and Table 4 for the *bulk growth model*). These relations link the time-growth mode λ to the wave-number k in an implicit way, as a function of the four dimensionless parameters β_i, σ, R^* and R_{out}. In particular, the parameters R^* and R_{out} define the geometrical properties of the system with respect to the diffusive length, l_c (*size* parameters), whereas β_i and σ are related to the mechanical and chemical characteristic of the system (*chemo-mechanical* parameters), as already discussed.

The dispersion curves obtained through the dispersion relation (26) are reported in Fig. 2 for different values of the size and chemo-mechanical parameters, for both the *chemotactic growth model* (solid lines) and the *bulk growth model* (dotted lines). Interestingly, no significant differences between the two models emerge in the linear stability analysis, and the colony front is found to be always unstable at small wavenumbers (i.e. large wavelengths). The prediction of an unstable expansion of a radial or planar bacterial colony was conjectured in [22], although not supported by any formal mathematical proof. Furthermore, the dispersion curves in Fig. 2 also demonstrate the emergence of a characteristic wavelengths in the development of instabilities. As expected, the surface tension acts a stabilizing effect on the front (see Fig. 2(a)): increasing the value of σ the characteristic unstable wavenumber decreases, as long as the mode related to $k = 1$ is the only unstable. Furthermore, the maximum amplification

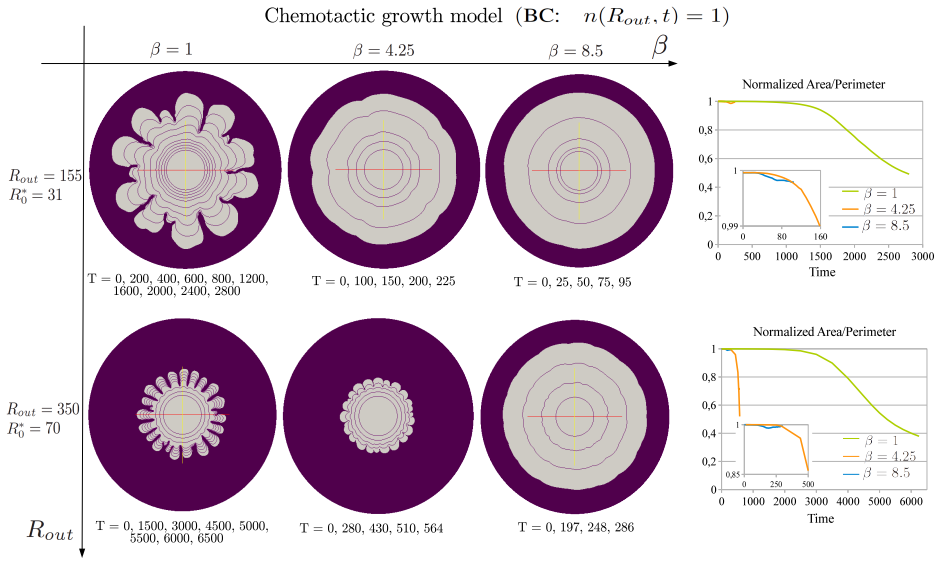

Figure 3: *Chemotactic growth model*: morphological diagram of pattern formation in bacterial colonies, obtained varying the model parameter β_1 and R_{out}, while keeping σ and R_{out}/R_0^* fixed ($\sigma = 0.007$, $R_{out}/R_0^* = 5$). The initial condition for the concentration of nutrients is equal to the solution of the quasi-stationary problem, given by (12). The profile of the colony is plotted for different instants of time (see below each contour plot for the specific values). The right charts show the area/perimeter ratio of the bacterial colony normalized with respect to the corresponding value for a circle (i.e. half of the averaged radius of the colony).

rate λ increases as β_i increases (as shown in Fig. 2(b)) and as the ratio between the radius of the Petri dish and the radius of the colony $q = R_{out}/R^*$ decreases (see Fig. 2(c)).
Since similar dispersion diagrams can be found in the study of non-living systems characterized by branching instabilities, such as in crystal growth problems [36], the dispersion curves in Fig. 2(a) suggest a strongly unstable expansion of the bacterial colony and the formation of branched patterns. In the next section we perform numerical simulations of both the system (1)-(4) and (1)-(5) in order to investigate the pattern formation in the nonlinear regime for the proposed models.

4 Numerical simulations

Numerical simulations for both the *chemotactic growth* and the *volumetric growth model* were obtained using a finite element code implemented using the software FreeFem++ [http://www.freefem.org], starting from an initial circular colony with radius $R^*(0) = R_0^*$. A triangular mesh with an adaptive time-scheme was used, in order to fit the moving boundary $\partial\Omega^-(t)$ at every time step.

Since the boundary condition (6) on $\partial\Omega^-(t)$ is required in order to solve for the pressure, the curvature C of the boundary is computed accordingly to the following

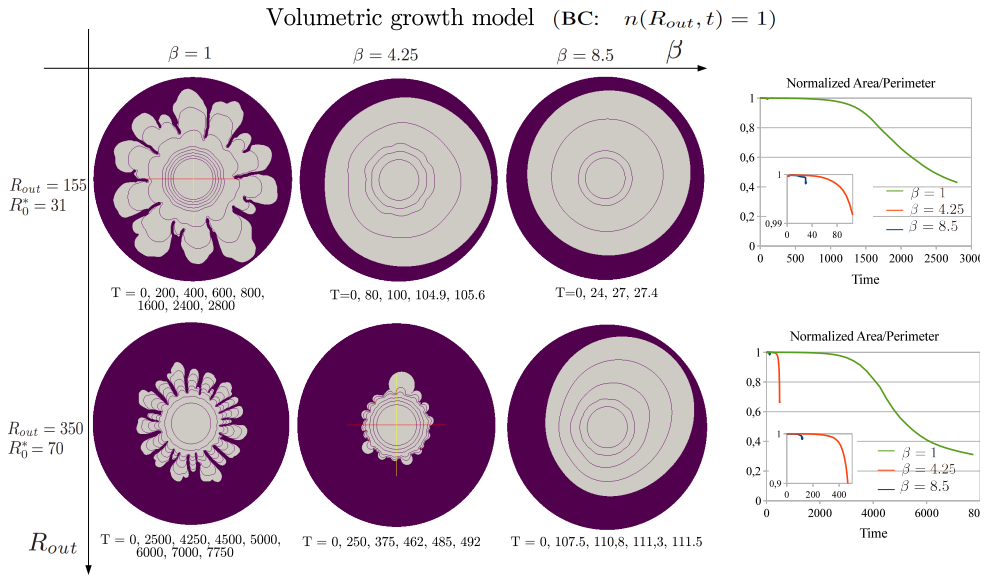

Figure 4: *Volumetric growth model*: bacterial colony contour plot for different values of the mechanical parameter β_2 and the size parameter R_{out}, keeping $\sigma = 0.007$ and $R_{out}/R_0^* = 5$ fixed. The initial condition for the concentration is given by Eq. (12). On the right charts we report the normalized area/perimeter ratio with respect to the corresponding value for a circle (i.e. half of the averaged radius of the colony).

relation $C = \mathrm{n}_y \mathrm{n}_x \mathrm{n}_{y,x} - \mathrm{n}_y^2 \mathrm{n}_{x,x} - \mathrm{n}_x^2 \mathrm{n}_{y,y} + \mathrm{n}_x \mathrm{n}_y \mathrm{n}_{x,y}$, where n_x and n_y are components of the normal $\mathbf{n}$ to the moving boundary along the Cartesian axes x and y and the comma denotes differentiation with respect to the argument. Then, a smoothing of the curvature is performed, by averaging over q_{smooth} near neighbours (in the simulations we set $q_{smooth} = 5$). A P2 finite element interpolation is performed to find an approximation of p_j on $\Omega^-(t)$, so that, once the pressure, p_j is known, it is possible to compute the velocity field, given by Eq. (3), through differentiation and determine the new position of the front at time t_{j+1}, using an explicit Euler time scheme. Finally, the diffusion equation for the nutrient (1) is solved using an implicit scheme in time. Another P2 finite element discretization is performed to find an approximation of n_{j+1} on $\Omega^-(t) \cup \Omega^+(t)$.

The developed simulation tool allowed studying the colonial shapes emerging in the non-linear regime using different dimensionless parameters in the model. We first performed a set of simulations varying β_i and R_{out}, while keeping R_{out}/R_0^* and σ fixed, considering the situation corresponding to the quasi-stationary analysis, i.e. boundary condition (10). The colony profiles at different instants of time are reported in the morphological diagrams in Fig. 3-left for the *chemotactic growth model* and Fig. 4-left for the *bulk growth model*, at different values of the dimensionless parameters β_i and R_{out}. Even if the theoretical analysis predicts that both models have a similar quasi-static dynamics, great discrepancies arise between the two models in the non-linear regime. In particular, for high values of β_2 in the *bulk growth model*, high asymmetries in the

colony profile are observed, whereas at intermediate values of β_2 a dynamical *blebbing* instability occurs at the colony boundary (see the contour plot obtained for $\beta_2 = 4.25$ and $R_{out} = 350$ in Fig. 4-left, for instance). The onset of asymmetries, which is generated by the nonlinear development of the linearly unstable mode $k = 1$, can be quantified in terms of translation in the center of mass of the colony. Hence, in Fig. 5 we report the finite displacements of the center of mass of the colony resulting from simulations of the *volumetric growth model*. On the other hand, such displacements are almost null in the case of the *chemotactic growth model*, since the Laplacian operator in Eq. (4) has a strong regularizing effect on instabilities characterized by small wave-numbers. The occurrence of asymmetric instabilities in the numerical simulations confirms the behavior pointed out by the linear stability analysis, in which for high values of the parameter β_2, the characteristic wavenumber of the perturbation is $k = 1$ (see Fig. 2(b)).

However, it is possible to observe from 4-left, that further decreasing the value of β_2, instabilities with small wavelengths develop also in the *volumetric growth model* and the asymmetries related to $k = 1$ are less pronounced, in agreement with the linear stability analysis.

The morphological diagrams in Figs. 3-left and 4-left also point out that the chemo-mechanical parameter β_i is linked to the onset of branching, with small values of β_i promoting the formation of fingers of decreasing thicknesses. Such small values of β_i correspond to situations in which the energy spent for the diffusion or the uptake of chemicals (in the chemotactic and volumetric growth model respectively) is predominant with respect to the energy converted in colony expansion, i.e. either the energy related to chemotaxis in the *chemotactic growth model* or the one due to mass production in the *volumetric growth model*. At the same time, since the velocity of the front expansion depends on β_i, both models predicts that low expansion velocities promote the development of contour instability at high wavenumbers, whereas fast front are more stable to small wavelength, that is a typical behaviour of growing living systems dominated by diffusion [7].

On the other hand, while β_i determines if branching occurs, the number of developing fingers is driven by the dimensionless radius R_{out}, at a fixed aspect ratio R_{out}/R_0^*. In particular, in Figs. 3-(left) and 4-(left) it is observed that smaller wavelength instabilities emerge as the size of the Petri dish increases with respect to the diffusive length l_c (i.e. higher values of R_{out}). The onset of branched patterns during colony evolution depends also on the other chemo-mechanical parameter of the model, σ, that stabilize small wave-length instabilities independently on the model used for the expansion of the colony. For instance, in Fig. 6 the evolution of the colony in the *bulk growth model* is reported, for different values of the dimensionless parameter σ. Being σ identified by the ratio between the surface tension of the bacterial colony and the friction between the colony and the medium, Fig. 6 states that either increased value of the colony surface tension, σ_b, or smaller friction coefficient will drive the expansion of rounded colonies.

Even though the morphological diagrams in Figs. 3-(left), 4-(left) and 6 qualitatively show the influence of size and chemo-mechanical parameters on pattern formation, a quantitative characterization of such patterns is needed. A good marker to deter-

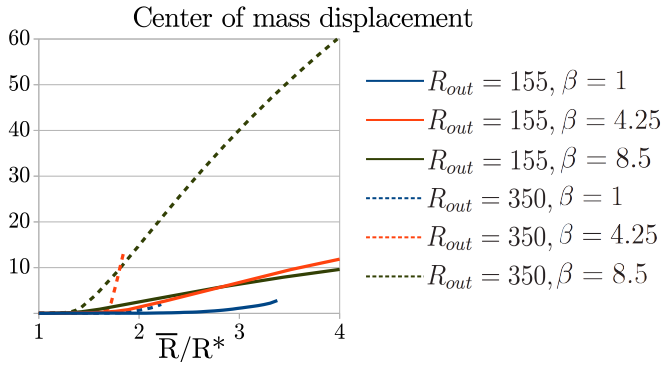

Figure 5: Measurements of the center of mass displacement over over the averaged radius of the colony, $\bar{R}$, normalized to the initial radius, R_0^*, for the *volumetric growth model*.

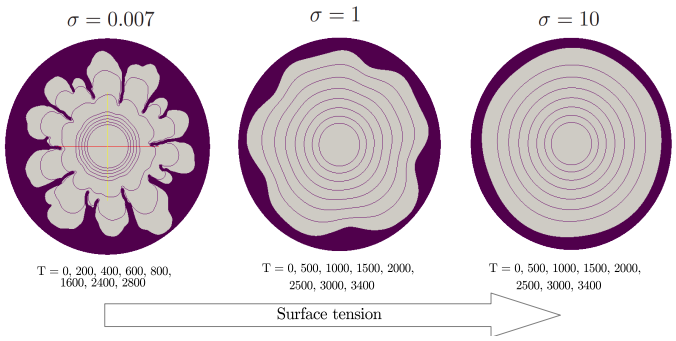

Figure 6: Influence of σ on the formation of contour instabilities, using the *volumetric growth model*. A stabilizing effect of the surface tension on the motion of the free boundary is also found in the *chemotactic growth model*.

mine the onset of the branching process is given by the plot of the area over perimeter ratio over time. In Fig. 3-right and Fig. 4-right) we report the area over perimeter ratio normalized with respect to the corresponding value for a circle, which is equal to half of the averaged radius of the colony. Therefore, the more branched the colony front the more the area over perimeter ratio differs from the value of 1, which identifies round colonies (Fig. 3-right and Fig. 4-right). Thus, the initial branching time can be easily identified from such plots, considering the instant of time at which the area over perimeter ratio significantly deviates from the value of 1.

Another important parameter to quantitatively characterize branched patterns is the *roughness* of the profile. The roughness is defined as the root of the mean square deviation of the local radius of the front from the average radius of the colony [14]. Both the local radius and the averaged radius are measured with respect to the center of mass of the colony, so that a translation of the center of mass will not give a contribution to the measured roughness. Fig. 7 reports the value of this parameter as a function of the averaged radius of the colony, $\bar{R}$, normalized to the initial radius, R_0^*, computed for

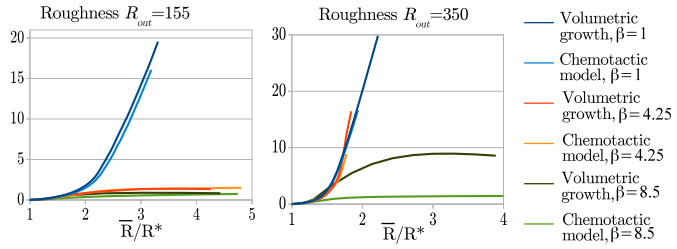

Figure 7: Roughness of the profiles reported in Fig.3 and 4 plotted over the ration between averaged radius of the colony, $\bar{R}$, and the initial radius, R_0^*.

the simulations shown in Fig. 3 and 4. It is possible to observe in both models that the roughness of the front saturates to an almost constant value in colonies that remains rounded, while for branched patterns it continuously increases as the colony expands.
However, we remark that neither the area over perimeter ratio nor the roughness of the profile point out differences between the two models, as they are not influenced by translations in the center of mass, which, as already observed, should be quantified directly, as in Fig. 5.
Let us now focus on the geometrical characteristics of the developing fingers (i.e. base and amplitude), referring to the numerical simulations in the upper-left of Figs. 3 and 4 (with $R_{out} = 155$, $R_0^* = 31$ and $\beta_i = 1$). The finger base is defined as the distance between two subsequent points of local maximum for the colony boundary curvature, whereas the amplitude of the finger is the maximum in the distance between the points belonging to the finger profile and the corresponding finger base vector.
Looking at the branched pattern reported in Figs. 3-(left), 4-(left) it is possible to see that the initially generated fingers may undergo further branching for giving rise to new fingers. We will call such structures as second generation fingers, as they occur from the splitting of the first appearing ones. Some of these second generation fingers remain very short, being limited by their neighbours, whereas others grow and they may undergo another splitting. In particular, both for the *volumetric growth model* and the *chemotactic growth* one, we observe that in the early stage (from $t = 650$ to $t = 1650$ in the *chemotactic growth model* and from $t = 500$ to $t = 1500$ in the *bulk growth model*) only five branches develop and then they split forming second generation fingers. Looking at the fingers' geometrical properties reported in Fig. 8-a for the *chemotactic growth model* and in Fig. 8-b for the *bulk growth model*, we observe that the amplitude and the base highly increase for the five initial fingers independently on the growth mechanism. Then, as soon as the second generation fingers appear, the base almost remain constant over time, whereas the amplitude strongly grows. The evolution of the base and amplitude can be represented by a power-law curve $c \cdot t^{\alpha}$, with fitting parameters c and α reported in Fig. 8-c and Fig. 8-d, for the *chemotactic growth* and *volumetric growth model* respectively. Surprisingly, we remark for both models that the best fitting exponent for the ratio amplitude/base of the fingers in the first stage is about 0.45, which is close to the square root growth exponent expected in

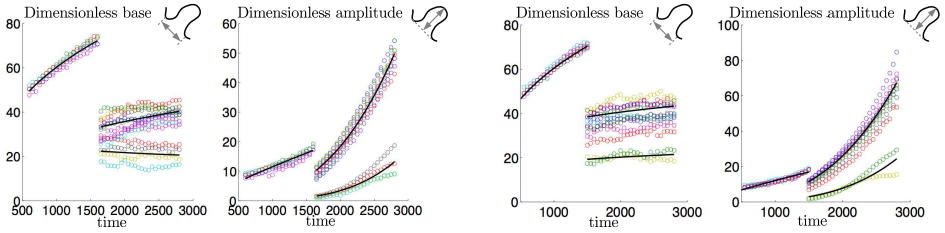

(a) (b)

Finger parameter	c	α
Base $t < 1650$	4.18	0.386
Amplitude $t < 1650$	0.036	0.83
Base $t \geq 1650$	71.23 (finer)	-0.1562 (finer)
	2.302 (bigger)	0.3609 (bigger)
Amplitude $t \geq 1650$	1.93E-13 (finer)	4.013 (finer)
	3.04E-9 (bigger)	2,963 (bigger)

(c)

Finger parameter	c	α
Base $t < 1500$	4.5	0.376
Amplitude $t < 1500$	0.039	0.83
Base $t \geq 1500$	5.45 (finer)	0.17 (finer)
	9.58 (bigger)	0.19 (bigger)
Amplitude $t \geq 1500$	4.7E-11 (finer)	3.4 (finer)
	128E-8 (bigger)	2,82 (bigger)

(d)

Figure 8: Finger base B and amplitude A, when $\beta_i = 1$, $R_{out} = 155$, $R_0^* = 31$, $\sigma = 0.007$. Using the *chemotactic growth model* (a) up to time $t = 1650$, five principal dendrites develop, then tip splitting occurs and 14 dendrites are recorded. On the other hand, in the *volumetric growth model* (b), tip splitting occurs before, at $t \approx 1500$. The table reports the fitting parameters of the data with a power-law curve of the kind ct^{α} (solid black lines) for (c) the *chemotactic growth model* and (d) the *volumetric growth model*.

instability processes dominate by diffusion [18].

Thus, even though branches appear earlier in the *volumetric growth model*, then the initial evolution of these branches is similar either if the colony expansion is driven by volumetric growth or by chemotaxis.

The results presented so far have been obtained considering an initially stationary concentration of nutrients and considering a fixed concentration of the chemicals at the outer boundary, which is the only case in which a quasi-stationary linear stability analysis can be performed. However, this condition might be valid only if the colony is sufficiently far from the border, if the nutrients are not continuously added. In biological experiments, the nutrients are introduced in the agar only at the beginning and, therefore, a null flux condition at the boundary of the Petri dish would be more realistic (i.e. eq. (11)). To study only the influence of the changed boundary condition on the

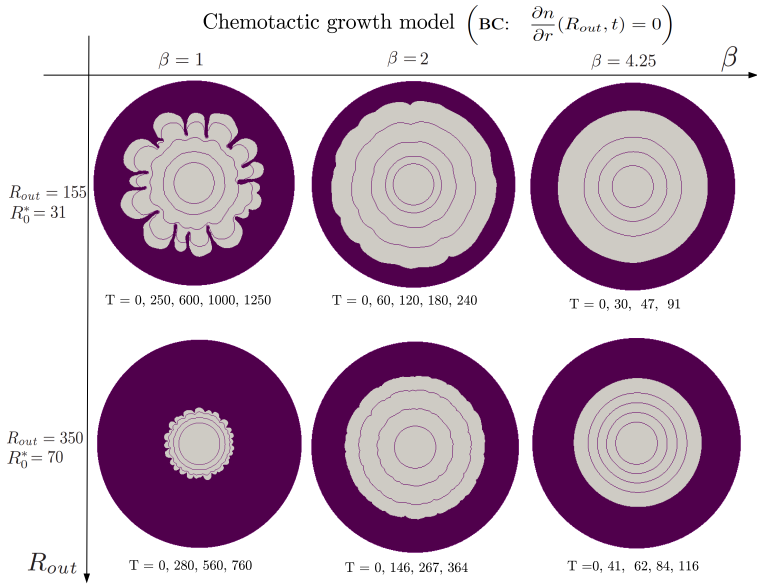

Figure 9: *Chemotactic growth model* with null flux boundary conditions: the bacterial colony contour plot is reported at different instants of time, for different values of the mechanical parameter β_1 and the size parameter R_{out}, while keeping $\sigma = 0.007$ and $R_{out}/R_0^* = 5$ fixed. The initial condition for the concentration is $c = 1$ everywhere. To start the simulations with a chemical gradient comparable with the one used in the simulations with the boundary condition given by Eq. (10), we let the nutrient field evolve for the first 100 instants of time, without letting the colony expand.

onset of instabilities, we let the nutrient field evolve for the first 100 instants of time, without letting the colony expand, in order to achieve at the beginning of the simulation a chemical gradient comparable to the one set in the simulations with Dirichlet boundary conditions. Thus we test our model under this new set of boundary and initial conditions, to check whether the obtained results can be extended also to this situation with more realistic BC. As done before, we perform a set of simulations, varying β_i and R_{out} (at R_{out}/R_0^* and σ fixed). The results obtained with this new set of BC are reported in Fig. 9, for the *chemotactic growth model*, and Fig. 10, for the *volumetric growth model*. From the new morphological diagrams, it is possible to state that the general rules previously outlined still hold: small values of the parameter β_i leads to the development of branches, whereas the number of branches that develop depends on the size parameters of the model. However, in this case, the velocity of the profile is faster and thus compact pattern with rough profile (in the chemotactic growth model) or translations in the center of mass of the colony (in the volumetric growth model) are reproduced setting lower values of the parameter β_i, with respect to the previous case (e.g $\beta_i = 1.5$ vs. $\beta_i = 4.25$). From the system dynamics reported in the morphological diagram, it is possible to highlight that the initial condition set in the simulations can be acceptable only in the case of branched patterns (i.e. small values of β_i), whereas in the case of round colony, the time required to the nutrients to create a significant chemical

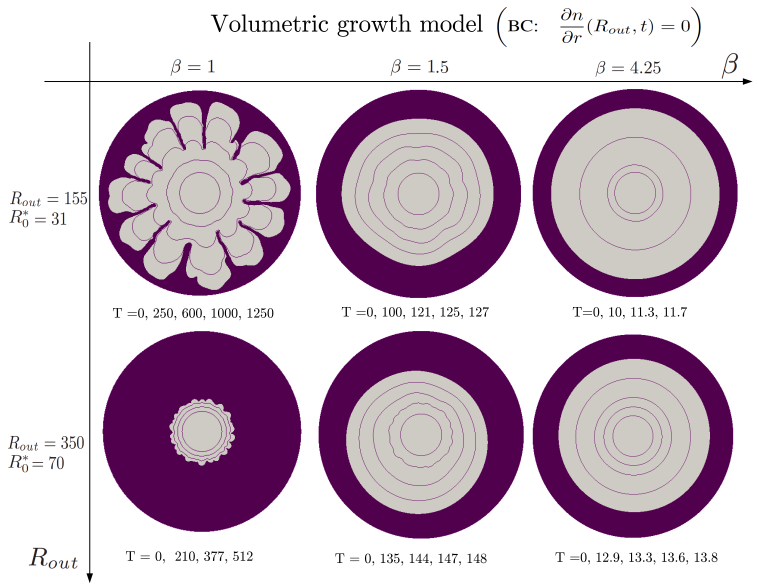

Figure 10: *Volumetric growth model* with null flux boundary conditions: morphological diagram reporting the bacterial colony contours at different instants of time, for different values of the parameter β_1 and R_{out}, while keeping $\sigma = 0.007$ and $R_{out}/R_0^* = 5$ fixed.

gradient is comparable to the time required for the colony expansion.

The results shown so far demonstrate that, independently on the boundary condition at the border of the Petri dish, both the *chemotactic growth* and the *bulk growth* model can reproduce different patterns, from rounded to branched ones, depending on the chemo-mechanical and size parameters, but even more important is to see in Fig. 11 the outstanding similarity between the morphologies predicted by our model and some of the patterns reported in literature for bacterial colonies.

Unfortunately, a direct quantitative comparison between the numerical simulations and the biological experiments shown in Fig. 11 is not straightforward, since not all the data required by the mathematical model are reported in the corresponding paper and since the model has been derived using several mathematical assumptions (such as constant and homogeneous bacterial density, quasi-stationary initial nutrient concentration, either linear volumetric or chemotactic expansion) that might not be valid in the biological experiments. Thus the comparison in the following should be regarded as a proof-of-concept to outline a biological interpretation of the mathematical results, without any intent to be a quantitative validation.

In particular, we showed that the *chemotactic growth model* is able to reproduce disk-like patterns (as the one in Fig. 11-a), using either high values of the chemo-mechanical parameter β_1 (see Fig. 11-f) or high values of the chemo-mechanical parameter σ (see Fig. 6-c). However, although disk-like colonies can be mathematically recovered by increasing σ, this would correspond to a ratio between the surface tension of the colony and the friction between the bacteria and the substrate that seems out of a biologically

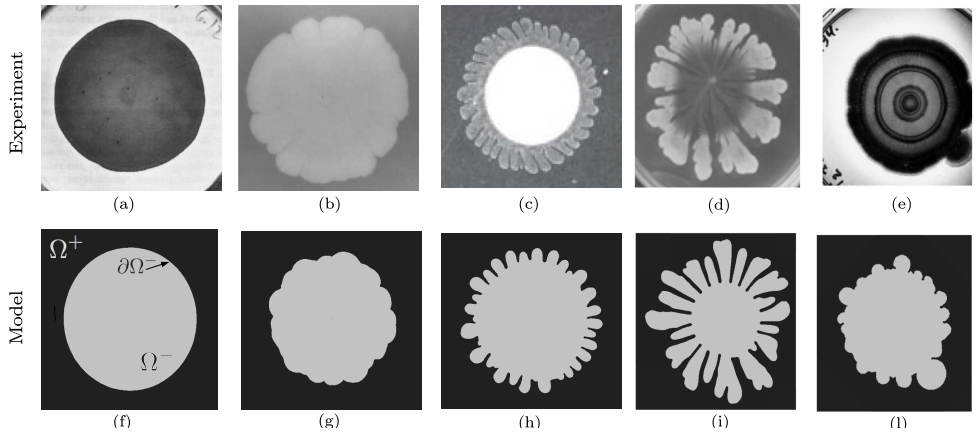

Figure 11: Comparison between some bacterial morphologies observed in biological experiments reported in the top figure (a)-(e), and the results obtained through the numerical simulations of the mechanical models proposed in this work, reproduced in the bottom figure, (f)-(l). Figures from biological experiments are reproduced, with permission, from (a) [29], (b) [42], (c) [5], (d) [46] and (e) [10]. The numerical simulations are obtained using the *chemotactic growth model* in (f)-(g)-(h) and the *volumetric growth model* in (i)-(l). The parameters setted in the experiments are: $\sigma = 0.007$ for all cases and (f) $R_0^* = 31$, $R_{out} = 155$ and $\beta_1 = 8.5$, (g) $R_0^* = 70$, $R_{out} = 350$, $\beta_1 = 8.5$, (h) $R_0^* = 100$, $R_{out} = 350$ and $\beta_1 = 1$, (i) $R_0^* = 70$, $R_{out} = 350$ and $\beta_1 = 0.5$, (l) $R_0^* = 70$, $R_{out} = 350$ and $\beta_2 = 4.25$.

admissible range, for the specific biological values reported for eukaryotic cells [6, 60]. Concerning the parameters set in the simulation in Fig. 11-f, a dimensionless external radius $R_{out} = 155$ will perfectly reproduce a Petri dish with standard radius of $44\,\mathrm{mm}$, considering a diffusion coefficient $D_n = 3 \cdot 10^{-11}\,\mathrm{m}^2/\mathrm{s}$ and an uptake rate $\gamma = 3.7 \cdot 10^{-4}\,\mathrm{s}^{-1}$, which are in the biological range [20, 24, 29, 58, 59] and that lead to a characteristic length $l_c \approx 285\,\mu\mathrm{m}$. Considering $\beta = 8.5$, as the one used in Fig. 11-f, we obtained an average velocity of the front equal to $\approx 3.2\,\mathrm{mm/h}$, which is in the order of magnitude of the values found in literature for round and compact colonies [33, 41].
An "Eden-like" pattern, as the one reported in Fig. 11-b [42], is reproduced by a *chemotactic growth model* with values of the parameter β_1 close to the one of disk-like patterns but higher values of the dimensionless parameter R_{out}, which corresponds to smaller characteristic diffusive lengths (or bigger Petri-dishes, which is not the case here). Thus patterns as the one in Fig. 11-b can be reproduced by our model considering a smaller diffusion coefficient $D_n = 10^{-11}\,\mathrm{m}^2/\mathrm{s}$ [29] and an uptake rate $\gamma = 6.5 \cdot 10^{-4}\,\mathrm{s}^{-1}$, that lead to a diffusive length $l_c \approx 125\,\mu\mathrm{m}$, compatible with the value $R_{out} \approx 350$ set in in Fig. 11-g. For such biological parameters, the characteristic velocity is $v_c \approx 290\,\mu\mathrm{m/h}$, that, in the case $\beta = 8.5$, leads to a mean front velocity of $136\,\mu\mathrm{m/h}$, which is in agreement with the velocities reported in litterature for such patterns [33, 41].
On the other hand, branched patterns such as the one reported in Fig. 11-c and Fig. 11-d can be obtained, both using the *chemotactic growth model* and the *volumetric growth model*: regular patterns with a high number of dendrites can be obtained using the

chemotactic growth model with small values of β_1 and high dimensionless external radius R_{out} (see Fig. 11-h), whereas asymmetric patterns with highly separated branches are reproduced by the *volumetric model* with really small values of β_2, as the one used in Fig. 11-i. In particular, the fingers' development and evolution reported in Fig. 11-c [5] are reproduced by our simulations in Fig. 11-h, considering $\gamma = 0.11 s^{-1}$ and $D_n = 10^{-10}\,\mathrm{m}^2/\mathrm{s}$ (i.e. $l_c \approx 30\,\mu\mathrm{m}$ and $t_c \approx 9\,\mathrm{s}$), so that the experimentally measured displacement of about $2.4\,\mathrm{mm}$ in the first 22 hours, for an colony with initial diameter of about $6\,\mathrm{mm}$ [5], is perfectly reproduced by the mathematical model with $R_0^* = 100$ and $\beta = 1$ (see Fig. 11-h), in which at time $T = 9000$ a displacement of $82 \cdot l_c$ is recorded. For what concerns the simulations obtained with the volumetric growth model, according to [29], the reproduction time of bacteria in optimal conditions (i.e. $n_c \approx 10\,\mathrm{g/l}$) is $25\,\mathrm{min}$giving a value of $K_\gamma = 6 \cdot 10^{-5}\,\mathrm{l}/(\mathrm{g}\cdot\mathrm{s})$. Moreover, in optimal nutrient concentration, biological experiments shows that colonies grow compact [29]. As in our model the compact expansion of the colony is obtained setting $\beta_2 \approx 8.5$, thanks to the definition of the dimensionless chemo-mechanical parameter, it is possible to derive $\gamma_n \approx 0.78 \cdot 10^{-4}\,\mathrm{s}^{-1}$, which is a reasonable biological uptake rate. Thus, a diffusion coefficient of $1.24 \cdot 10^{-12}\mathrm{m}^2/\mathrm{s}$ will lead to a diffusive length $l_c \approx 125\,\mu\mathrm{m}$, which is suitable to describe standard Petri dishes of radius $44\,\mathrm{mm}$. Considering these values for the diffusion coefficient (even though below the admissible biological range), uptake rate and reproduction frequency, the value of $\beta_2 = 0.5$ settled in Fig. 11-i corresponds to a nutrient concentration $n_c \approx 0.65\,\mathrm{g/l}$, which is close to the range reported in [29] for highly branched patterns, whereas the value of $\beta_2 = 4.25$ correspond to a nutrient concentration $n_c \approx 5.52\,\mathrm{g/l}$, in agreement with the concentration found in biological experiments for dense branched patterns and compact ones [29]. Moreover, for such intermediate values of β_2 coupled with high values of R_{out}, the model predicts the onset of blebbing instabilities in the colony profile (see Fig. 11-l), similarly to the one reported in Fig. 11-e [10].
For the sake of completeness, we remark that, being the nutrients' diffusion coefficient inside the water $D_n = 10^2 - 10^3\,\mu m^2/s$, the quasi-stationary assumption used to obtain the initial nutrient concentration might be properly formulated only in the case of slowly growing colonies, such as branched and Eden-like patterns, that develop with a speed of $\approx 1.5 \cdot 10^{-2} - 10^{-1}\,\mu m/s$ [5, 33, 41]. On the other hand, circular colonies expand with a front speed of approximately $1 - 5\,\mu m/s$ [33,41], thus the time required to fill the Petri-dish might be of the same order of the time required to reach the chemical equilibrium. Thus in this case an initial quasi-stationary concentration seems not a good guess of the biological condition. However circular patterns can also be obtained with the same model, without imposing the initial quasi-stationary condition for the nutrients, starting from a homogeneous condition for the chemicals.

5 Discussion

In this work we proposed a continuum model for describing the onset and the nonlinear development of contour instabilities in an initially circular and homogeneous bacterial

colony. The nutrient distribution is described using a standard reaction-diffusion equation, so that the local bacterial growth on the Petri dish depends on nutrient availability. Two mechanisms for the expansion of the colony are considered: we either assume that mass accretion is due to a non-convective mass flux inside the colony, which is proportional to the chemical gradient (*chemotactic growth model*), or we consider a bulk mass supply (*volumetric growth model*). In both cases, the expansion of the colony satisfies the mass and momentum balances for the bacteria, together with the required boundary conditions at the free moving interface.

The equation systems describing the dynamic of the colony are characterized by four dimensionless parameters, two of them (β_i and σ) describing the *chemo-mechanical* interactions whilst the other ones (R_0^* and R_{out}) take into account the *size* properties of the system. In particular, the parameter β_i represents the ratio of conversion of the energy provided by the nutrient into the energy which makes the colony expand (i.e. either chemotactic expansion or volumetric mass production), whereas σ measures the ratio between the surface tension of the colony and the friction with the substrate. On the other hand, the size parameters take into account the relative dimension of the colony and of the Petri-dish with respect to the diffusive length.

The modelling approach proposed here differs from previous continuous ones, e.g. [42,43], for the introduction of a sharp interface representing the colony contour, for the consideration of both mechanical, chemical and size effects and for the direct comparison of two possible mechanisms driving the expansion of the colony, i.e. chemotaxis vs. volumetric growth.

The two proposed models are studied using both analytical and computational tools. First, a linear stability analysis (Section 3.2) is performed for both models, pointing out that the initially circular colony is always unstable at high wave-lengths, with typical dispersion curves found for branching processes in non-living systems [36]. Second, numerical simulations have been performed using a finite element scheme (see Section 4), proving the onset of branched patterns in the nonlinear regime. In particular, numerical results have confirmed the existence of a characteristic wavenumber, predicted by the analytical analysis, whilst they have shown striking differences (see Figs. 3 and 4) between the chemotactic vs. volumetric growth mechanisms, highlighting the emergence of asymmetries and blebbing instabilities in the *volumetric growth model*.

The development of numerical tools has also allowed to investigate the influence of the chemo-mechanical and size parameters on the pattern formation, under more realistic boundary conditions that cannot be studied through the perturbation of the quasi stationary solution (e.g. the null flux BC at the border of the Petri dish). Notably, the computational analysis points out that the chemo-mechanical parameters trigger the onset of the developing instability whereas the size parameters determine the typical wavelength of the developing fingers. Indeed, we prove that high values of the surface tension (or equivalently small value of the friction coefficient, i.e. high σ) and elevated front velocities (i.e. high β_i) stabilize the expanding colony, confirming the experimental observations that compact patterns arise for fast expanding colonies, whereas branched ones occur for slowly moving fronts [41]. On the other hand, the typical wave-lengths of the possible instability is dictated by the size parameters: smaller wave-lengths instabilities

occur for decreasing ratios between the diffusive length and the dimension of the Petri dish.

The resulting patterns are also quantitatively characterized through measurements of the area over perimeter ratio of the colony, the roughness of the profile, the aspect ratio of the developing fingers and the translation of the center of mass. In particular, the evolution of the area over perimeter ratio and the roughness plots allowed determining the branching onset, whereas the initial scaling of fingers' aspect ratio demonstrates that the process is governed by diffusion at an early stage [18]. Although these parameters are similar for the two expansion mechanisms, the measurements of the translation in the center of mass identifies great dissimilarities between the two models. In particular, this analysis suggests that asymmetries mostly relies on a volumetric bacteria production rather than on chemotactic movements. In fact, the chemotactic expansion is less sensitive to perturbations with small wavenumbers and, thus, translations in the center of mass of the colony are not appreciable in the numerical simulations.

Finally, we show that the proposed models, although kept as simple as possible, are able to qualitatively reproduce some of the patterns observed during biological experiments (see Fig. 11), which range from disk-like patterns to more ramified ones depending on the model parameters chosen. However, despite the striking qualitative agreement between our simulations and the experimental patterns, quantitative tests are highly needed to verify whether the right biological features are included in the modelling approach and to improve the model. Future work will focus on the investigation of the colony expansion by introducing nonlinear constitutive equation for the chemotactic and volumetric growth terms which could better fit some experimental results, i.e. showing a Monod-type dynamics.

Furthermore, the assumptions of the present model make it suitable to describe the experimental expansion observed for bacterial monolayers in microffluidic experiments, such as the one perfomed in [55]. Conversely, a limitation arises in those cases where the bacterial density is inhomogeneous, e.g. concentric ring like pattern. However, we remark that the model can be numerically implemented, with slightly changes, considering a time and space varying density described by the mass conservation equation of the bacterial colony. Finally, we considered separate contributions for volumetric growth and mass fluxes, whereas in the biological set-up the two mechanisms coexist. Therefore, even though this work is useful to establish the separated effects of each of the two mechanisms on the formation of branches, future models should focus on the combination of volumetric growth and chemotactic motion, as done for instance in [19].

In conclusion, despite the simplifications introduced, this work demonstrates that the formation and dynamical evolution of patterns in microbial colonies is the result of a sophisticated interplay among mechanical, chemical and size parameters of the system. Indeed the morphological diagrams presented in Fig. 3 and Fig. 4 propose a new interpretation on the emergence of branched patterns, relating contour instabilities of the colony to chemo-mechanical and size parameters, rather than on the concentration of the chemicals and of the agar, as the other morphological diagrams proposed in literature [14, 26, 41–43]. Moreover, differently from previous models, the branching

Table 3: Perturbed pressure field p_1 and dispersion relation for the surface flux model.

	Chemotactic growth model
$\lambda \neq \{0, -1\}$	$p_1(r) = Er^k - \beta_1 A I_k(\sqrt{\lambda+1}r)$ $E = \frac{1}{R^{*k}}\left(\frac{\sigma}{R^{*2}}(k^2-1) + \beta_1 n_0 \frac{I_1(R^*)}{I_0(R^*)} + \beta_1 A I_k(\sqrt{\lambda+1}R^*)\right)$ $\lambda = -\frac{\sigma}{R^{*3}}k(k^2-1) + \beta_1 A\sqrt{\lambda+1} I_{k+1}(\sqrt{\lambda+1}R^*) - \beta_1 n_0 \left((1+k)\frac{I_1(R^*)}{R^* I_0(R^*)} - 1\right)$
$\lambda = 0$	$p_1(r) = E_0 r^k - \beta_1 A_0 I_k(\sqrt{\lambda+1}r)$ $E_0 = \frac{1}{R^{*k}}\left(\frac{\sigma}{R^{*2}}(k^2-1) + \beta_1 n_0 \frac{I_1(R^*)}{I_0(R^*)} + \beta_1 A_0 I_k(\sqrt{\lambda+1}R^*)\right)$ $\lambda = -\frac{\sigma}{R^{*3}}k(k^2-1) + \beta_1 A_0\sqrt{\lambda+1} I_{k+1}(\sqrt{\lambda+1}R^*) - \beta_1 n_0 \left((1+k)\frac{I_1(R^*)}{R^* I_0(R^*)} - 1\right)$
$\lambda = -1$	$p_1(r) = (E_1 - \beta_1 A_1) r^k$ $E_1 = \frac{1}{R^{*k}}\left(\frac{\sigma}{R^{*2}}(k^2-1) + \beta_1 n_0 \frac{I_1(R^*)}{I_0(R^*)} + \beta_1 A_1 R^{*k}\right)$ $\lambda = -\frac{\sigma}{R^{*3}}k(k^2-1) - \beta_1 n_0 \left((1+k)\frac{I_1(R^*)}{R^* I_0(R^*)} - 1\right)$

structures are obtained without resorting on either a non-linear diffusion coefficient, as in [33, 43] or the definition of a passive state for bacteria, as in [41] or the inclusion of ad-hoc non-linearities in the production, chemotactic and consumption terms.
Thus, our models give an insight on the role played by physical forces in guiding morphological processes in living aggregates, and it might be applied application with appropriate refinements to the description of other biological relevant problems, such as wound-healing [25, 39, 44, 45, 49] and biofilm formation [20, 51].

Appendix

In Section 3.2, the linear stability analysis applied to the quasi-stationary problem lead to the definition of the dispersion equation in the compact form (26), as a function of the unperturbed and perturbed pressure field. Here, we report some details on how eq. (25) and (26) have been obtained and the specific expressions for the perturbed pressure and the dispersion equations in the *chemotactic growth model* (Table 3) and in the *bulk growth model* (Table 4). The boundary conditions (25) for the perturbed pressure at the interface, can be easily obtained, provided that (6) should hold, therefore

$$p(R^* + \varepsilon e^{\lambda t}\cos(k\theta)) = p_0 - \sigma_b C(R^* + \varepsilon e^{\lambda t}\cos(k\theta))\,. \tag{27}$$

Table 4: Perturbed pressure field p_1 and dispersion relation for the *volumetric growth model*.

	Bulk growth model
$\lambda \neq \{0,-1\}$	$p_1(r) = Er^k - \frac{\beta_2 A}{\lambda+1} I_k(\sqrt{\lambda+1}r)$
	$E = \frac{1}{R^{*k}}\left(\frac{\sigma}{R^{*2}}(k^2-1) + \beta_2 n_0 \frac{I_1(R^*)}{I_0(R^*)} + \frac{\beta_2 A}{\lambda+1} I_k(\sqrt{\lambda+1}R^*)\right)$
	$\lambda = -\frac{\sigma}{R^{*3}}k(k^2-1) + \frac{\beta_2 A}{\sqrt{\lambda+1}} I_{k+1}(\sqrt{\lambda+1}R^*) - \beta_2 n_0\left((1+k)\frac{I_1(R^*)}{R^* I_0(R^*)} - 1\right)$
$\lambda = 0$	$p_1(r) = E_0 r^k - \frac{\beta_2 A_0}{\lambda+1} I_k(\sqrt{\lambda+1}r)$
	$E_0 = \frac{1}{R^{*k}}\left(\frac{\sigma}{R^{*2}}(k^2-1) + \beta_2 n_0 \frac{I_1(R^*)}{I_0(R^*)} + \frac{\beta_2 A_0}{\lambda+1} I_k(\sqrt{\lambda+1}R^*)\right)$
	$\lambda = -\frac{\sigma}{R^{*3}}k(k^2-1) + \frac{\beta_2 A_0}{\sqrt{\lambda+1}} I_{k+1}(\sqrt{\lambda+1}R^*) - \beta_2 n_0\left((1+k)\frac{I_1(R^*)}{R^* I_0(R^*)} - 1\right)$
$\lambda = -1$	$p_1(r) = E_1 r^k - \frac{\beta_2 A_1}{4(k+1)} r^{k+2}$
	$E_1 = \frac{1}{R^{*k}}\left(\frac{\sigma}{R^{*2}}(k^2-1) + \beta_2 n_0 \frac{I_1(R^*}{I_0(R^*)} + \frac{\beta_2 A_1}{4(k+1)} R^{*k+2}\right)$
	$\lambda = -\frac{\sigma}{R^{*3}}k(k^2-1) + \frac{\beta_2 A_1}{2(k+1)} R^{*k+1} - \beta_2 n_0\left((1+k)\frac{I_1(R^*)}{R^* I_0(R^*)} - 1\right)$

Computing the curvature of the perturbed interface and considering on both sides only the first order terms, the following relation holds

$$p^*(R^*) + \varepsilon e^{\lambda t}\cos(k\theta)\left(\frac{\partial p^*}{\partial r}(R^*) + p_1(R^*)\right) \approx p_0 + \sigma_b\left(\frac{1}{R^*} + \varepsilon e^{\lambda t}\cos(k\theta)\frac{1}{R^*}(k^2-1)\right). \quad (28)$$

The derivation of (25) is then straightforward.
In a similar way the dispersion equation (26) can be retrieved imposing the boundary condition (7) at the perturbed interface and neglecting the terms of order higher than the first, in the series expansion.
The coefficient A, A_0, A_1 can be found in Table 2 and they are the same for both models. As it is evident from Tables 3 and 4, the dispersion equations link the time-growth mode λ to the wave-number k in an implicit way, as a function of the four dimensionless parameters β_i, σ, R^* and R_{out}.

References

[1] Friedl P., Hegerfeldt Y., Tusch M., "Collective cell migration in morphogenesis and cancer." *Int. J. Dev. Biol.* 48, 441-449 2004

[2] Adler J (1966) "Chemotaxis in bacteria." *Science* 153, 708-716.

[3] Ambrosi D, Athesian GA, Arruda EM, Cowin SC, Dumais J, Goriely A, Holzapfel GA, Humphrey JD, Kemkemer R, Kuhl E , Olberding JE Taber LA and Garikipati

K (2011) “Perspectives on growth and remodeling.” *J. Mech. Phys. Solids* 59(4), 863-883.

[4] Bassler BL and Losick R (2006) “Bacterially speaking.” *Cell* 125, 237-246.

[5] Be’er A, Zhang HP, Florin EL, Payne SM, Ben-Jacob E and Swinney HL (2009) “Deadly competition between sibling bacterial colonies.” *PNAS* 106, 428-433.

[6] Ben Amar M (2013) “Chemotaxis migration and morphogenesis of living colonies.” *Eur. Phys. J. E. Soft Matter* 36 (6), doi: 10.1140/epje/i2013-13064-5.

[7] Ben Amar M, Chatelain C and Ciarletta P (2011) “Contour Instabilities in Early Tumor Growth Models.” *Phys. Rev. Lett.* 106, 148101.

[8] Ben-Jacob E (1993) “From snowflakes formation to growth of bacterial colonies. Part I: Diffusive patterning in azoic systems.” *Contemp. Phys.* 34: 247-273.

[9] Ben-Jacob E (1997) “From snowflakes formation to growth of bacterial colonies II: Cooperative formation of complex colonial patterns.” *Contemp. Phys.* 38 (3), 205 - 241.

[10] Ben-Jacob E, Cohen I and Gutnick DL (1998) “Cooperative organization of bacterial colonies: from genotype to morphotype.” *Annu. Rev. Microbiol.* 52, 779-806.

[11] Ben-Jacob E, Cohen I and Levine H (2000) “Cooperative self-organization of microorganisms.” *Adv. Phys.* 49, 395-554.

[12] Ben-Jacob E, and Levine H (2006) “Self-engineering capabilities of bacteria.” *J. R. Soc. Interface* 3, 197-214.

[13] Ben-Jacob E and Schultz D (2010) “Bacteria determine fate by playing dice with controlled odds.” *PNAS* 107, 13197-13198.

[14] Bonachela JA, Nadell CD, Xavier JB, and Levin SA (2011) “Universality in Bacterial Colonies.” *J. Stat. Phys.* 144 (2), 303-315.

[15] Cerretti F, Perthame B, Schmeiser C, Tang M and Vauchelet N (2010) “Waves for a hyperbolic Keller-Segel model and branching instabilities.” *Math. Models Methods Appl. Sci.* 21.

[16] Ciarletta P, Ambrosi D and Maugin GA (2012) “Mass transport in morphogenetic processes: a second gradient theory for volumetric growth and material remodeling.” *J. Mech. Phys. Solids* 60(3), 432-450.

[17] Ciarletta P (2012) “Free boundary morphogenesis in living matter.” *Eur. Biophys. J.* 41, 681-686.

[18] Cross MC and Hohenberg PC (1993) “Pattern formation outside of equilibrium.” *Rev. Mod. Phys.* 65.

[19] Croze OA, Ferguson GP, Cates ME, Poon WC (2011) "Migration of chemotactic bacteria in soft agar: role of gel concentration." *Biophys J.* 101 (3), 525-534.

[20] Dockery J and KlapperI (2001) "Finger formation in biofilm layers." *SIAM J. Appl. Math.* 62(3), 853-869.

[21] Eden M (1961) "A two-dimensional growth process." *Fourth Berkeley Symp. on Math. Statist. and Prob.* 4, 223-239.

[22] Farrell FDC, Hallatschek O, Marenduzzo D and Waclaw B (2013) "Mechanically driven growth of quasi-two dimensional microbial colonies." *Phys. Rev. Lett.* 111, 168101.

[23] Flemming HC, Wingender J (2010) "The biofilm matrix." *Nature Rev.* 8, 623-633.

[24] Ford RM and Lauffenburger DA (1991) "Analysis of chemotactic bacterial distributions in population migration assays using a mathematical model applicable to steep or shallow attractant gradients." *Bull. Math. Bio.* 53, 721-749.

[25] Friedl P, Hegerfeldt Y and Tusch M (2004) "Collective cell migration in morphogenesis and cancer." *Int. J. Dev. Biol.* 48, 441-449.

[26] Fujikawa H and Matsushita M (1989), "Fractal Growth of Bacillus subtilis on Agar Plates." *J. Phys. Soc. Jap.* 58 (11), 3875-3878.

[27] Fujikawa H (1994) "Diversity of the Growth Patterns of Bacillus Subtilis Colonies on Agar Plates." *FEMS Microbiol. Ecol.* 13, 159-168.

[28] Ganghoffer JF (2010) "Mechanical modeling of growth considering domain variation - Part II: Volumetric and surface growth involving Eshelby tensors." *J. Mech. Phys. Solids* 58, 1434-1459.

[29] Golding I, Kozlovsky Y, Cohen I and Ben-Jacob E (1998) "Studies of bacterial branching growth using reaction-diffusion models for colonial development." *Physica A* 260, 510-554.

[30] Guyon E, Hulin JP, Petit L and De Gennes PG (2001) "Hydrodynamique physique." *EDP sciences Les Ulis*, France.

[31] Hamill OP and Martinac B (2001) "Molecular Basis of Mechanotransduction in Living Cells." *Phys. Rev.* 81(2), 685-740.

[32] Humphrey JD (2003) "Continuum biomechanics of soft biological tissues." *Proc. R. Soc. London A* 459, 3-46.

[33] Kawasaki K, Mochizuki A, Matsushita M, Umeda T and Shigesada N (1997) "Modeling Spatio-Temporal Patterns Generated by Bacillus subtilis." *J. Theor. Biol.* 188, 177185.

[34] Keller EF and Segel LA, (1971), "Model for chemotaxis." *J. Theor. Biol.* 30, 225-234.

[35] Kozlovsky Y, Cohen I, Golding I, Ben-Jacob E (1999) "Lubricating bacteria model for branching growth of bacterial colony." *Phys. Rev. E. Phys. plasmas fluids Relat. Interdiscip. Topics* 50, 7025-7035.

[36] Langer JS (1980) "Instabilities and pattern formation in crystal growth." *Rev. Mod. Phys.* 52 (1), 1-30.

[37] Lecuit T and Lenne PF (2007) "Cell surface mechanics and the control of cell shape, tissue patterns and morphogenesis." *Nat. Rev. Mol. Cell. Biol.* 8, 633-644.

[38] Manz BN and Groves JT (2010) "Spatial organization and signal transduction at intercellular junctions." *Nat. Rev. Mol. Cell Biol.* 11 , 342-352.

[39] Mark S, Shlomovitz R, Gov NS, Poujade M, Grasland-Mongrain E and Silberzan P (2010) "Physical model of thedynamic instability in an expanding cell culture." *Biophys. J.* 98, 361-370.

[40] Marrocco A, Henry H, Holland IB, Plapp M, Sé ror SJ and Perthame B, (2010) "Models of self-organizing bacterial communities and comparisons with experimental observations." *Math. Model. Nat. Phenom.* 5(1), 148-162.

[41] Matsushita M, Wakita J, Itoh H, Ràfols I, Matsuyama T, Sakaguchi H and Mimura M (1998) "Interface growth and pattern formation in bacterial colonies." *Physica A* 249, 517-524.

[42] Matsushita M, Hiramatsu F, Kobayashi N, Ozawa T, Yamazaki Y, and Matsuyama T (2004) "Colony formation in bacteria: experiments and modeling." *Biofilms* 1, 305-317.

[43] Mimura M, Sakaguchi H, and Matsushita M (2000) "Reaction-diffusion modelling of bacterial colony patterns." *Physica A* 282, 283-303.

[44] Nikolić DL, Boettiger AN, Bar-Sagi D, Carbeck JD and Shvartsman SY (2006) "Role of boundary conditions in an experimental model of epithelial wound healing." *Am. J. Physiol. Cell Physiol.* 291, 68-75.

[45] Nobes CD and Hall A (1999) "Rho GTPases Control Polarity, Protrusion, and Adhesion during cell movement." *J. Cell. Biol.* 144, 1235-1244.

[46] O'May C and Tufenkji N (2011) "The swarming motility of Pseudomonas aeruginosa is blocked by Cranberry Proanthocyanidins and other tannin-containing materials." *Appl. Environ. Microbiol.* 77, 3061-3067.

[47] Parent CA and Devreotes PN (1999) "A cells sense of direction." *Science* 284, 765-770.

[48] Paterson, L (1981) "Radial fingering in a Hele-Shaw cell." *J. Fluid Mech.* 113, 513-529.

[49] Poujade M, Grasland-Mongrain E, Hertzog A, Jouanneau J, Chavrier P, Ladoux B, Buguin A and Silberzan P (2007) "Collective migration of an epithelial monolayer in response to a model wound." *PNAS* 104 (41), 15988-15993.

[50] Saffman PG and Taylor G (1958) "The penetration of a fluid into a medium or hele-shaw cell containing a more viscous liquid." *Proc. Soc. London*, Ser A, 245, 312-329.

[51] Seminara A et al. (2012) "Osmotic spreading of Bacillus subtilis biofilms driven by an extracellular matrix." *PNAS* 109, 1116-1121.

[52] Shapiro JA (1988) "Bacteria as Multicellular Organisms." *Sci. Am.* 258, 82-89.

[53] Taber LA (1995) "Biomechanics of growth, remodeling, and morphogenesis." *Appl. Mech. Rev.* 48, 487-545.

[54] Tindall MJ, Maini PK, Porter SL and Armitage JP (2008) "Overview of Mathematical Approaches Used to Model Bacterial Chemotaxis II: Bacterial Populations." *Bull. Math. Bio.* 70, 1570-1607.

[55] Volfson D, Cookson S, Hasty J and Tsimring LS (2008) "Biomechanical Ordering of Dense Cell Populations." *PNAS* 105 (40), 15346-15351

[56] Wakita J, Komatsu K, Nakahara A, Matsuyama T and Matsushita M (1994) "Experimental investigation on the validity of population dynamics approach to bacterial colony formation." *J. Phys. Soc. Jap.* 63, 1205-1211.

[57] Wakita J, Itoh H, Matsuyama T and Matsushita M (1997) "Self-Affinity for the Growing Interface of Bacterial Colonies." *J. Phys. Soc. Jap.* 66(1), 67-72.

[58] Yu SR, Burkhardt M, Nowak M, Ries J, Petrášek Z, Scholpp S, Schwille P and Brand M (2009) "Fgf8 morphogen gradient forms by a source-sink mechanism with freely diffusing molecules." *Nature* 461(7263), 533-537.

[59] Zhou S, Lo WC, Suhalim JL, Digman MA, Gratton E, Nie Q and Lander AD (2012) "Free Extracellular Diffusion Creates the Dpp Morphogen Gradient of the Drosophila Wing Disc." *Current Biology* 22, 668-675.

[60] Ziebert F and Aranson IS (2013) "Effects of adhesion dynamics and substrate compliance on the shape and motility of crawling cells." *PLoS One* 8 , e64511.

MOX Technical Reports, last issues

Dipartimento di Matematica
Politecnico di Milano, Via Bonardi 9 - 20133 Milano (Italy)

45/2015 Lange, M.; Palamara, S.; Lassila, T.; Vergara, C.; Quarteroni, A.; Frangi, A.F.
Improved hybrid/GPU algorithm for solving cardiac electrophysiology problems on Purkinje networks

44/2015 Antonietti, P.F.; Houston, P.; Smears, I.
A note on optimal spectral bounds for nonoverlapping domain decomposition preconditioners for hp-Version Discontinuous Galerkin methods

43/2015 Deparis, S.; Forti, D.; Gervasio, P.; Quarteroni, A.
INTERNODES: an accurate interpolation-based method for coupling the Galerkin solutions of PDEs on subdomains featuring non-conforming interfaces

42/2015 Brugiapaglia, S.; Nobile, F.; Micheletti, S.; Perotto, S.
A theoretical study of COmpRessed SolvING for advection-diffusion-reaction problems

41/2015 Quarteroni, A.; Veneziani, A.; Vergara, C.
Geometric multiscale modeling of the cardiovascular system, between theory and practice

40/2015 Patelli, A.S.; Dedè, L.; Lassila, T.; Bartezzaghi, A.; Quarteroni, A.
Isogeometric approximation of cardiac electrophysiology models on surfaces: an accuracy study with application to the human left atrium

39/2015 Guglielmi, A.; Ieva, F.; Paganoni, A.M.; Quintana, F.A.
A semiparametric Bayesian joint model for multiple mixed-type outcomes: an Application to Acute Myocardial Infarction

38/2015 Grasso, M.; Menafoglio, A.; Colosimo, B.M.; Secchi, P.
Using Curve Registration Information for Profile Monitoring

37/2015 Aletti, M.; Perotto, S.; Veneziani, A.
Educated bases for the HiMod reduction of advection-diffusion-reaction problems with general boundary conditions

36/2015 Fedele, M.; Faggiano, E.; Barbarotta, L.; Cremonesi, F.; Formaggia, L.; Perotto, S.
Semi-Automatic Three-Dimensional Vessel Segmentation Using a Connected Component Localization of the Region-Scalable Fitting Energy